A bimetallic benzene-1,2,4,5-tetrathiolate (btt) molybdenocene complex Cp2Mo(btt)MoCp2: radical and diradical states

Khalil Youssef, Corentin Poidevin, Antoine Vacher, Yann Le Gal, Oscar Charpentier, Marc Fourmigué, Arnaud Fihey, Frédéric Barrière, Thierry Roisnel, Dominique Lorcy

Chemistry–A European Journal
Research Article
doi.org/10.1002/chem.202300584
Chemistry Europe
European Chemical Societies Publishing
www.chemeurj.org

A Bimetallic Benzene-1,2,4,5-Tetrathiolate (btt) Molybdenocene Complex $Cp_2Mo(btt)MoCp_2$: Radical and Diradical States

Khalil Youssef,[a] Corentin Poidevin,[a] Antoine Vacher,[a] Yann Le Gal,[a] Oscar Charpentier,[a] Marc Fourmigué,[a] Arnaud Fihey,[a] Frédéric Barrière,[a] Thierry Roisnel,[a] and Dominique Lorcy*[a]

Abstract: Benzene-1,2,4,5-tetrathiolate (btt) has been used as a bridging ligand to prepare a redox active (molybdenocene dithiolene)-based bimetallic complex $Cp_2Mo(btt)MoCp_2$, which exhibits four successive electron transfers up to the tetracation. Spectro-electrochemical investigations together with DFT and TD-DFT calculations evidence that the two electroactive MoS_2C_2 metallacycles are electronically coupled in the monocationic as in the dicationic state. Two salts of the dication $[Cp_2Mo(btt)MoCp_2]^{2+}$ have been structurally characterized with PF_6^- and HSO_4^- counterions, showing different chair or boat conformations associated with variable folding angles of the two MoS_2C_2 metallacycles along the S–S hinge. The bis-oxidized dicationic complex exhibits a diradical character, with both radicals essentially localized on the metallacycles and with antiferromagnetic coupling evidenced from magnetic susceptibility measurements.

Introduction

Tetrathiolate ligands where two dithiolene moieties are connected through an organic linker are interesting precursors for the formation of functional polymeric materials exhibiting either conducting or attractive optical properties upon oxidation (Scheme 1a),[1,2,3] a consequence of their non-innocent character.[4] Among the few ligands used as precursors of such linear coordination polymers, 1,2,4,5-benzenetetrathiolate (btt) has been also investigated as precursor of *isolated bimetallic* complexes (Scheme 1b), $L_nM(btt)ML_n$, with a variety of metallic centers (M = Fe,[5] Ni and Pd,[6] Au,[7] Cr,[8] Ti, Zr and Hf,[9] Co,[10] Rh and Ir).[11] Such complexes can be considered as models of the linear coordination polymers, albeit their isolation in oxidized forms is still a challenge. Indeed, only two mono-oxidized salts have been reported so far, based on the nickel[6b] or chromium[8] bimetallic complexes shown in Scheme 1c.

Bis(cyclopentadienyl)molybdenum(IV) dithiolene (dt) complexes, $Cp_2Mo(dt)$, are an interesting family of redox active, $18e^-$, d^2 complexes which can be reversibly oxidized to the radical cation and the dication species.[12,13,14] When two such electroactive $Cp_2Mo(dt)$ moieties are linked through a conjugated organic spacer (Scheme 2a), electronic interplay might occur along the spacer which can be detected by electrochemistry through the occurrence of multi redox systems and

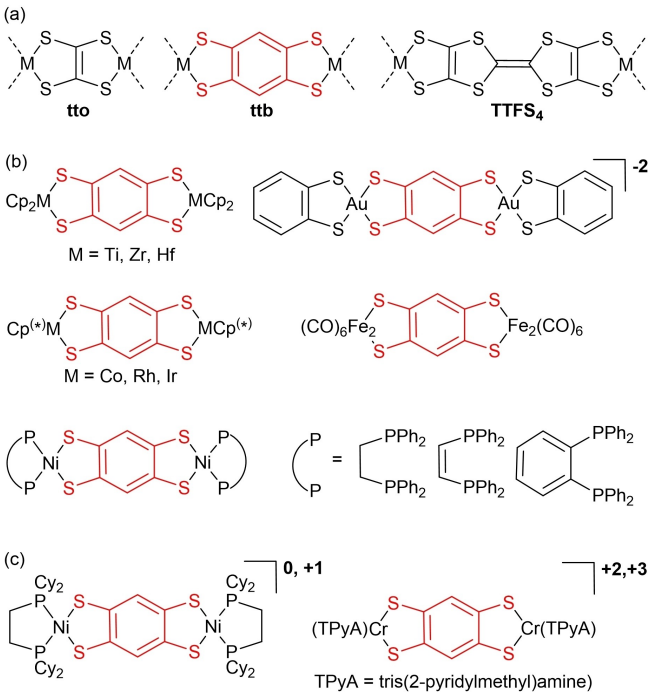

Scheme 1. (a) Tetrathiolate ligands involved in linear coordination polymers. (b) Bimetallic complexes reported to date involving the benzene-1,2,4,5-tetrathiolate (btt) ligand, highlighted in red. (c) Known mono-oxidized complexes.

[a] K. Youssef, Dr. C. Poidevin, Dr. A. Vacher, Y. L. Gal, O. Charpentier, Dr. M. Fourmigué, Dr. A. Fihey, Dr. F. Barrière, Dr. T. Roisnel, Prof. Dr. D. Lorcy
Université de Rennes, CNRS
ISCR (Institut des Sciences Chimiques de Rennes) - UMR 6226
35000 Rennes (France)
E-mail: dominique.lorcy@univ-rennes1.fr

Supporting information for this article is available on the WWW under https://doi.org/10.1002/chem.202300584

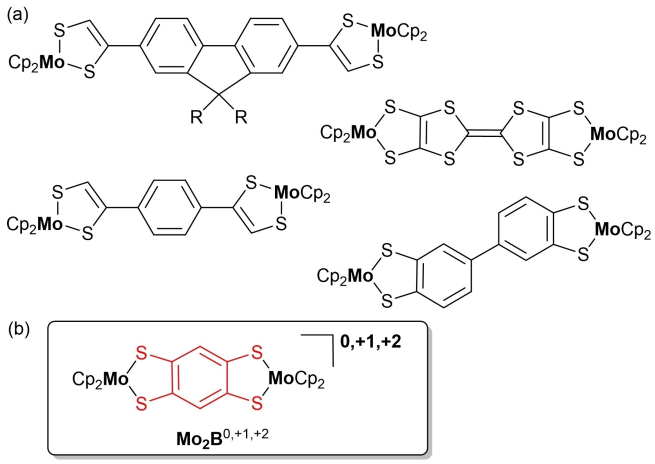

Scheme 2. (a) Known bimetallic molybdenocene dithiolene complexes and (b) the target **Mo_2B** complex.

by spectroelectrochemistry through the appearance of an intervalence charge transfer band in the near-IR region.[15] Several examples were reported with various extent of conjugation between the two centers, but no oxidized species has been isolated so far.

We therefore considered the shorter and conjugated btt ligand to build the original corresponding bimetallic complex, namely $Cp_2Mo(btt)MoCp_2$ (abbreviated as **Mo_2B**), in order to investigate the role of the benzo group as a linker between the two redox-active MoS_2C_2 metallacycles (Scheme 2b). We present here the synthesis of this bimetallic complex, **Mo_2B**, together with its optical, redox, and electronic properties through electrochemical and spectrochemical investigations. DFT calculations shed light on the nature of the absorption bands and on the structure of the neutral and oxidized forms of the complex, **Mo_2B^+** and **Mo_2B^{2+}**. Two crystal structures of the dicationic species **Mo_2B^{2+}** are reported (with different counter-ions and different conformations of the complex) and the electronic nature of the **Mo_2B^{2+}** diradical[16] is discussed.

Results and Discussion

The target complex, **Mo_2B**, was prepared starting from the proligand **1**, 1,3,5,7-tetrathia-*s*-indacene-2,6-dione[17] (Scheme 3).

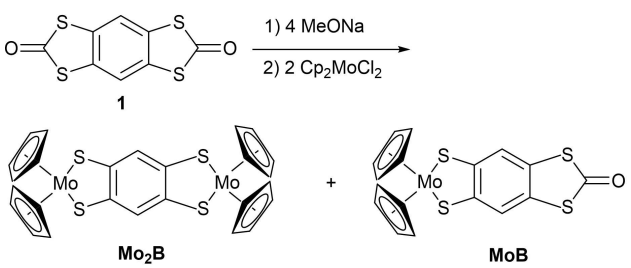

Scheme 3. Synthesis of the metallocene complexes **Mo_2B** and **MoB**.

The bimetallic complex **Mo_2B** was isolated in 43% yield, together with 10% of monometallic molybdenocene complex **MoB** (Scheme 3).

While **Mo_2B** is too insoluble in most solvents to obtain single crystals amenable to structure resolution, crystals of the mononuclear complex **MoB** were obtained by slow concentration of a dichloromethane solution. **MoB** crystallizes in the monoclinic system, space group $P2_1/c$. The structure (Figure 1a) is characterized by a weak folding of the metallacycle along the S1–S2 axis by $\theta = 10.4(2)°$. In addition, we also re-investigated the structure of a model compound with 1,2-benzenedithiolate (bdt) ligand, i.e. $Cp_2Mo(bdt)$, for comparison purposes (Figure 1b).[18] Apart from the S1–S2 hinge which is more pronounced in the case of **MoB** (10.4° for **MoB** vs 8.3° for $Cp_2Mo(bdt)$), the bond lengths and angles of the benzo moieties and the metallacycles are similar in both **MoB** and $Cp_2Mo(bdt)$ complexes.

The two btt complexes, **MoB** and **Mo_2B**, have been studied by cyclic voltammetry (CV) in CH_2Cl_2, together with $Cp_2Mo(bdt)$ (Table 1). Since **Mo_2B** is poorly soluble in CH_2Cl_2, all complexes were also investigated in DMSO, even if the potential window for anodic scans is notably smaller. Both mononuclear complexes, **MoB** and $Cp_2Mo(bdt)$ exhibit two reversible oxidation waves corresponding to the successive oxidation to the radical cation and the dication (Figure 2 for **MoB** and Figure S1 for $Cp_2Mo(bdt)$). When the experiment was performed in DMSO (Figures S1 and S2), the second oxidation process is not reversible anymore but the oxidation potentials compare with those determined in CH_2Cl_2. The anodic shift (140 mV) of the first oxidation potential of **MoB** (+0.42 V vs SCE) vs. $Cp_2Mo(bdt)$ (+0.28 V vs SCE) demonstrates the electron withdrawing effect of the fused dithiole-2-one ring in **MoB**.

The bimetallic complex, **Mo_2B**, exhibits a notably different voltammogram (Figure 2), with now three redox processes with similar peak current intensity. The two first ones are fully reversible while the third oxidation process is not, most presumably because of adsorption of the oxidized species at the electrode. The presence of three redox systems with close peak current intensity is unexpected for the coexistence of two redox active $Cp_2Mo(dithiolene)$ moieties in the same molecule. Indeed, if they were to behave independently, the two redox active moieties should be oxidized near-simultaneously and

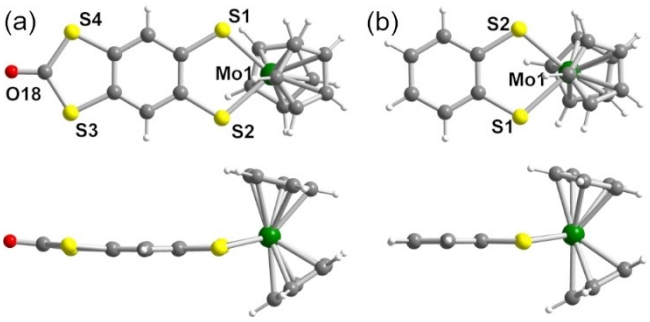

Figure 1. Top and side views of the monometallic (a) **MoB** and (b) $Cp_2Mo(bdt)$ complexes.

Table 1. Half-wave redox potentials[a] and ΔEp[b] of investigated complexes (E in V vs SCE).

Complexes	Solvent	$E^1_{1/2}$ (ΔEp)	$E^2_{1/2}$ (ΔEp)	$E^3_{1/2}$ (ΔEp)	E^4_{peak}
MoB	CH_2Cl_2	+0.42 (70)	+1.08 (60)		
	DMSO	+0.43 (60)	+1.01*		
$Cp_2Mo(bdt)$	CH_2Cl_2	+0.28 (60)	+1.02 (70)		
	DMSO	+0.31 (60)	+0.93*		
Mo_2B	CH_2Cl_2	-0.13 (60)	+0.37(60)	+1.09 (130)	
	DMSO	-0.03 (60)	+0.38 (70)		
(from Mo_2B^{2+} salt)	CH_3CN	-0.09 (60)	+0.34 (60)	+1.05 (60)	+1.57

[a] Oxidation processes, taken as the average of the anodic and the cathodic peak potentials. [b] ΔEp (in mV): peak-to-peak separation. *Irreversible process.

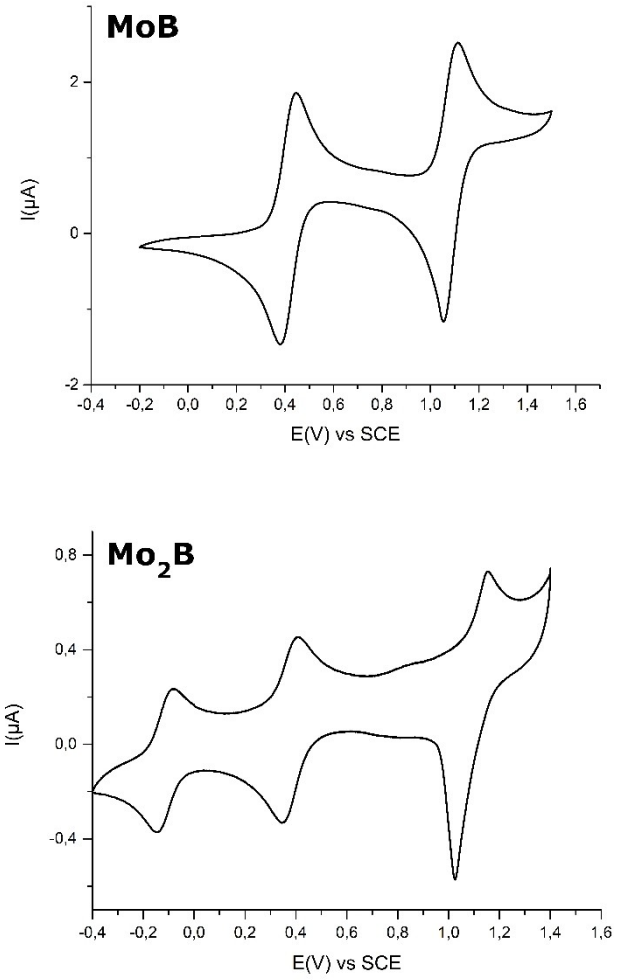

Figure 2. Cyclic voltammogram of **MoB** and **Mo_2B** in CH_2Cl_2 0.1 M Bu_4NPF_6 scan rate 100 mV/s, E inV vs SCE.

only two redox processes of similar intensity should be observed. Otherwise, four successive redox processes of similar intensity would be expected, as observed with dimeric tetrathiafulvalenes (TTF) where the two redox-active TTFs are fused to a benzo spacer group.[19] This indicates that the expected fourth redox process in **Mo_2B** probably occurs outside the CH_2Cl_2 electroactivity domain. The CV of **Mo_2B** in DMSO (Figure S2) shows only two redox processes due to the smaller potential window of DMSO vs. CH_2Cl_2. The presence of two Cp_2Mo(dithiolene) moieties in **Mo_2B** induces a very strong cathodic shift of 410 mV of the first redox potential ($E^1_{1/2} = -0.13$ V vs SCE) when compared with that of monometallic reference complex $Cp_2Mo(bdt)$ ($E^1_{1/2} = +0.28$ V vs SCE). The presence of the second electron rich metallacycle in **Mo_2B** induces an increase in the overall electron density of the dinuclear complex compared to the mononuclear one, $Cp_2Mo(bdt)$.

Spectroelectrochemical investigations

In order to determine the UV-vis-NIR signatures of the different redox states, spectroelectrochemical investigations were carried out in CH_2Cl_2 for **MoB** and $Cp_2Mo(bdt)$, but in DMSO for **Mo_2B**, with 0.2 M Bu_4NPF_6 as supporting electrolyte. The neutral *monometallic* complexes exhibit absorption bands only in the UV-vis range with the lowest energy band centered at 460 nm in **MoB** (Figure 3) and at 472 nm in $Cp_2Mo(bdt)$, close to that observed for analogous monometallic molybdenocene dithiolene complexes.[12,20] It is assigned to a ligand-to-metal charge transfer transition (LMCT) between the dithiolene ligand and the molybdenum center. Upon gradual oxidation, this LMCT transition gradually decreases and new absorption bands in the UV-vis region centered at 552 nm (**$MoB^{+\bullet}$**) and 402 nm [$Cp_2Mo(bdt)^{+\bullet}$] grow as well as a broad band centered in the NIR region at 1066 nm and 1027 nm for **$MoB^{+\bullet}$** (Figure 3) and $Cp_2Mo(bdt)^{+\bullet}$ (Figure S3) respectively. This evolution upon oxidation is the one typically observed in all the mononuclear Cp_2Mo(dithiolene) complexes with this lowest energy band in the range 1040–1150 nm.[12,13,20] Upon oxidation to the dicationic state this broad adsorption band in the NIR disappears (Figure S3).

Turning now to the bimetallic **Mo_2B** complex, since it is easily oxidized in air, we first reduced the solution to the neutral state through an electrolysis at −0.4 V vs. SCE during 15 min before performing the spectroelectrochemical investigation upon oxidation. Upon gradual oxidation (Figure 4a), besides the gradual disappearance of the band localized at 550 nm, new absorption bands in the UV-visible region at 330,

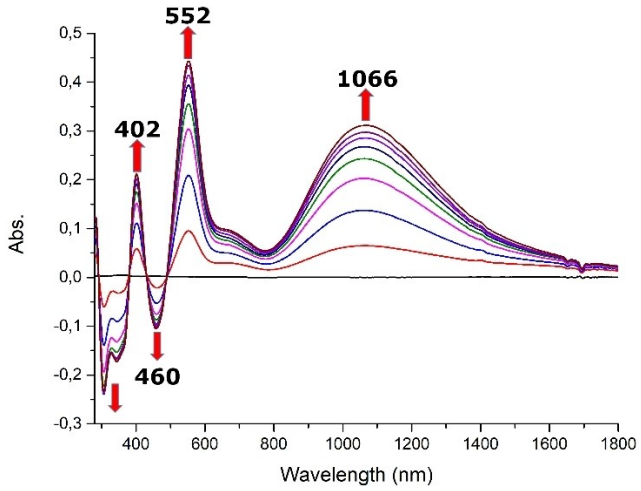

Figure 3. Differential UV-vis-NIR absorption spectra of **MoB**, monitored from the neutral to the radical cation state.

414 nm and in the NIR range at 836, 936, 1234 and 1444 nm are growing. Then, upon oxidation to the second oxidation step (Figure 4b), the intensity of the absorption band at 1444 nm slightly diminishes while a novel band centered at 1204 nm increases together with the appearance of a novel band centered at 711 nm. The shape of these spectra in the NIR range is rather complex when compared with other bimetallic molybdenocene complexes (Scheme 2) connected by a notably longer organic spacer.[15] Similar spectroelectrochemical experiments were realized in DMF (Figure S4) but besides a small hypsochromic shift of the adsorption bands, the evolution of the spectra upon gradual oxidation remains the same, indicating that the shape of the spectra is not due to an interaction with DMSO. In the NIR range for example, the band at 1432 nm in DMF is found at 1444 nm in DMSO and that at 1187 nm in DMF is found at 1204 nm in DMSO.

DFT calculations

Density functional theory calculations provide additional insight into the spectra evolution occurring during the spectroelec-

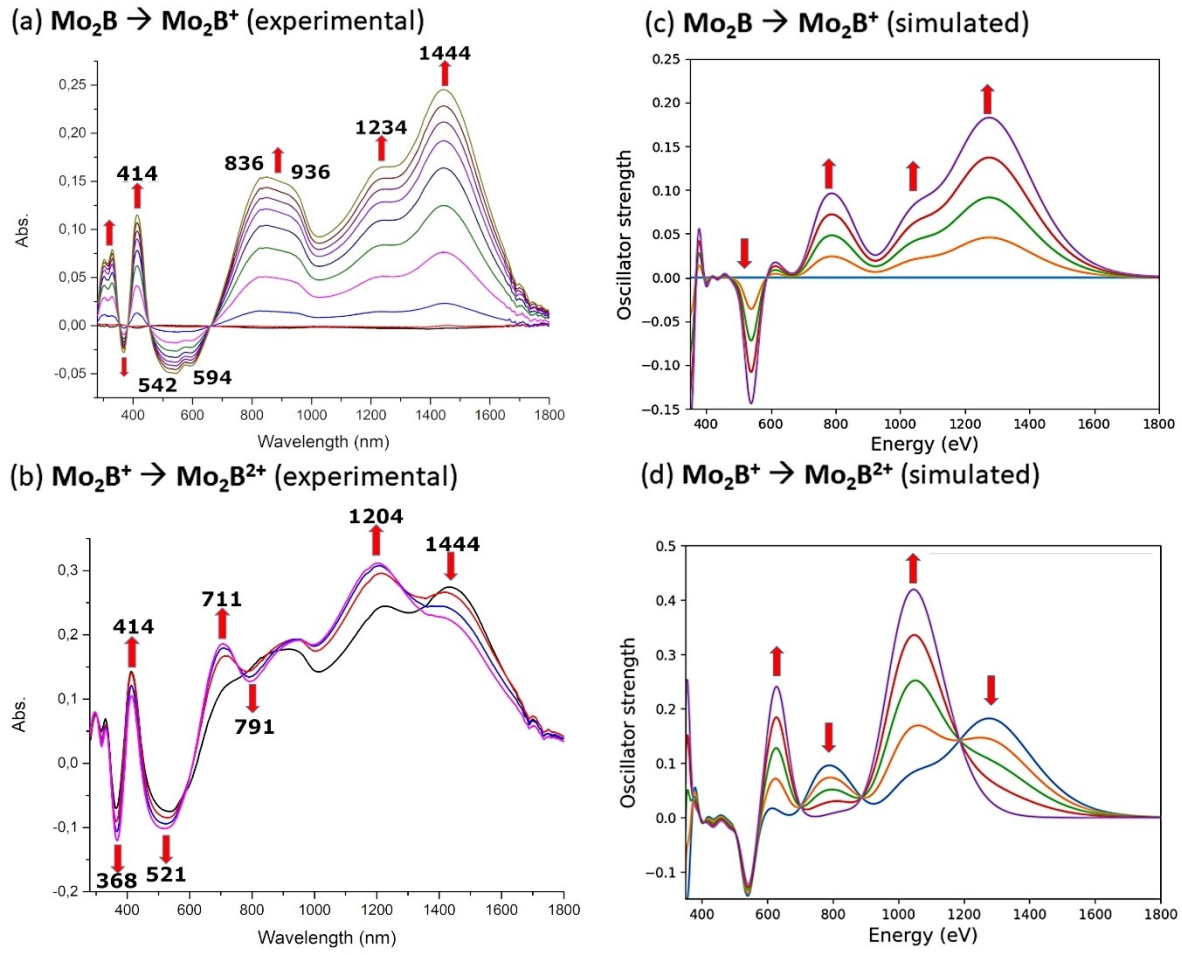

Figure 4. Experimental (a,b) and simulated (c,d) differential UV-vis-NIR absorption spectra of **Mo_2B**, monitored from neutral to radical cation state (a,c), from radical cation to dication state (b,d).

trochemical experiment carried out on **Mo_2B**. The geometry optimization of the ground state of the neutral **Mo_2B** structure leads to unfolded MoS_2C_2 metallacycles, as reported in all neutral monometallic $Cp_2Mo(dt)$ complexes,[12–15] and also observed here in **MoB** and $Cp_2Mo(bdt)$ (Cf. Figure 1). The simulated UV-visible spectrum of **Mo_2B** with a peak at 542 nm (Figure 5a, blue line) is in good agreement with the experimental low-energy absorption centered at 550 nm (Figure 4a). This absorption is dominated by a HOMO→LUMO transition corresponding to a LMCT transition (see charge density difference plot in Figure S5). For the mono-oxidized **$Mo_2B^{+\bullet}$** radical species, three minimal-energy conformers were found, a quasi-planar structure, a "boat" structure and a "chair" structure (see Figure 5a). The planar structure is calculated to be the most stable by only 3.6 kJ/mol and 4.6 kJ/mol compared to the boat and the chair conformers, respectively. These small relative energy differences are within the error of the DFT computational method, thus all three structures are considered to coexist experimentally at room temperature. The calculated UV-visible-NIR spectrum of each conformer (Figure 5a) exhibits two dominant bands in the NIR. All structures have similar absorption profile, though the boat and the chair conformers exhibit bands that are slightly red shifted for the lowest peak and blue shifted for the second peak with respect to the planar conformer.

The charge density differences between the excited states responsible for these absorption bands and the ground state (Figure S6) confirm that the transitions are of the same MLCT nature for all three conformers and for both transitions. To simulate the differential UV-vis-NIR absorption spectra when going from the neutral **Mo_2B** to the mono-oxidized **$Mo_2B^{+\bullet}$**, a weight of one third was used on the intensities of the three conformers and the resulting calculated differential spectrum is shown in Figure 4c. The progressive oxidation of the neutral molecule is modeled through four spectra that are produced with consecutive increments of 25% of the monocationic differential signature. The main features of the *experimental* differential UV-vis-NIR spectrum shown in Figure 4a are very well reproduced by our calculations (Figure 4c), lending strong support to the coexistence of the different conformers in solution.

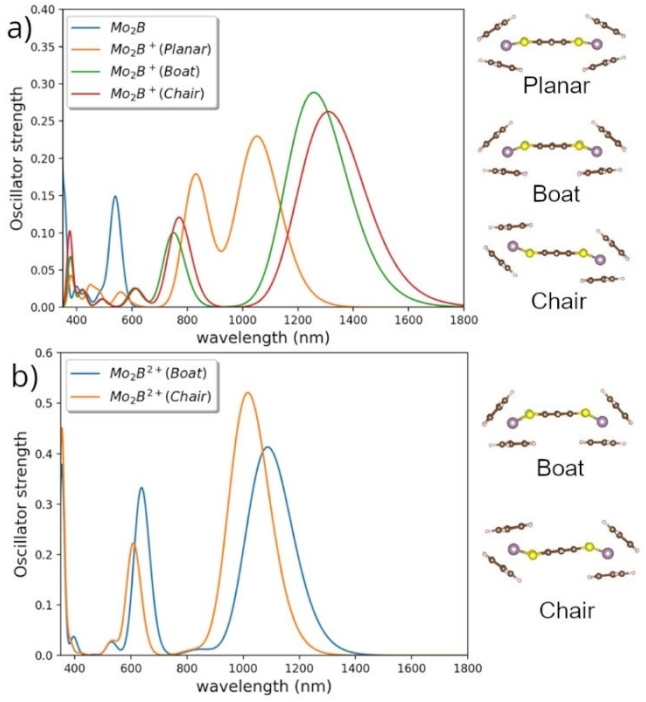

Figure 5. Simulated UV-vis-NIR spectra of (a) **Mo_2B** and **$Mo_2B^{+\bullet}$** and (b) **Mo_2B^{2+}** with a representation of the different conformers of **$Mo_2B^{+\bullet}$** and **Mo_2B^{2+}**.

For the di-cationic **Mo_2B^{2+}**, two quasi-degenerated conformers were found, corresponding to a boat and a chair structure (Figure 5b). The computed absorption spectra of the two conformers of **Mo_2B^{2+}** are found to be similar, with a band in the NIR and one in the visible region (Figure 5b). The simulation of the differential UV-vis-NIR spectrum between the mono-oxidized (including the three conformers) and the bis-oxidized (including the two conformers with a $^1/_2$ weight) species is produced following the procedure described above and is shown in Figure 4d. The main experimental features (Figure 4b) are here also well reproduced with a slight blue shift of the absorption bands, and a growth of bands centered at 800 and 1300 nm, to be compared with the experimental values at 711 and 1204 nm.

The optimized geometries show, upon oxidation of **Mo_2B**, an increase of the folding of the MoS_2C_2 metallacycles along the S–S axis (see Table S1), from essentially flat metallacycles in neutral complexes to folding angles predicted in the range 9–24° in mono-oxidized complexes, in the range 25–31° in dicationic ones. Concomitantly, a lengthening of the C–C bond within the metallacycle, a shortening of the other C–C bonds of the benzene ring and a shortening of the C–S bonds is predicted (Table S1). We thus anticipate an evolution from an aromatic benzene ring to a "quinonoid" form as the charge of the complex increases. This observation correlates well with the analysis of the atomic charges of the systems (Table S2). Indeed, for the first two oxidation states, **$Mo_2B^{+\bullet}$** and **Mo_2B^{2+}**, the main atomic charge differences are observed on the S atoms and to a lesser extent on the Mo atoms.

If we compare now within the same redox state the influence of the conformation, we can notice some differences between the planar and the non-planar boat and chair conformations of **$Mo_2B^{+\bullet}$**, especially on the metallacycles (Table S1). For instance, the shortening of the C–S bonds and the lengthening of the C=C bond are more pronounced in the case of the unfolded structure compared to the boat or chair folded conformations. This effect has been already noticed in mononuclear $[Cp_2Mo(dmit)]^{+\bullet}$ complexes isolated with different anions and exhibiting different folding angles of the metallacycle.[14a] The computed spin densities of the three conformers (Figure 6) are however very similar except for a slight increase on the metals for the non-planar structures. They are mainly delocalized on the four S atoms as well as on the π system of the central ring.

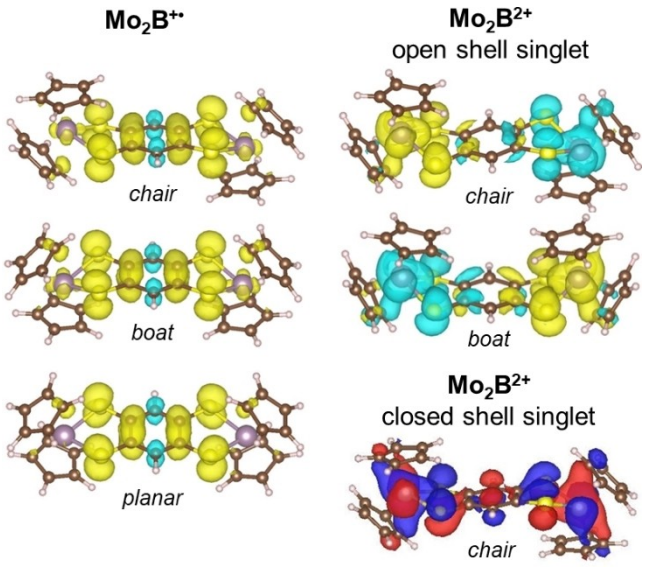

Figure 6. Spin density plots of $\mathbf{Mo_2B^{+\bullet}}$ and $\mathbf{Mo_2B^{2+}}$(open shell singlet), as well as the HOMO of the closed shell singlet of $\mathbf{Mo_2B^{2+}}$.

The triplet state of $\mathbf{Mo_2B^{2+}}$ is found 18 kJ/mol higher in energy than the closed shell singlet and is thus not expected to be observed experimentally. In addition, calculations on the broken symmetry solutions of $\mathbf{Mo_2B^{2+}}$ at both conformations (boat and chair), and after spin decontamination using Yamaguchi procedure[21] at the triplet geometries, show that both calculated structures are found to be more stable in the open shell singlet state (by about 5 kJ/mol compared to the closed shell singlet). However, the low calculated energy difference between the closed shell and the open shell singlet state could indicate the coexistence of the two electronic configurations. For the broken symmetry solutions of the bis-oxidized system, $\mathbf{Mo_2B^{2+}}$ (boat and chair), the spin densities are partially delocalized on the S atoms and Mo centers of the metallacycles with negligible contributions on the central ring for both conformers much like the HOMO of the closed shell singlet solutions (Figure 6).

The excellent agreement between calculated and experimental optical properties confirms the observation of the monocationic and dicationic species by spectroelectrochemistry and demonstrates that the folding angle of the metallacycles should increase with the degree of oxidation of the bimetallic complex. To further validate these assumptions, **Mo_2B** was oxidized chemically to isolate the corresponding dication, as detailed in the following.

Structural and electronic properties of the dication

The chemical oxidation of **Mo_2B** was performed in concentrated sulfuric acid in the air, by analogy to the procedure reported to oxidize ferrocene to ferrocenium.[22] After stirring overnight, the solution was poured into an aqueous solution of KPF_6. A dark green precipitate was isolated after filtration. Most of this precipitate is soluble at room temperature in acetonitrile while a residue is partially soluble in hot acetonitrile. Crystals were obtained by slow concentration of the CH_3CN-soluble fraction at room temperature. These dark green crystals were analyzed as the PF_6^- salt of the dicationic complex, $(\mathbf{Mo_2B})(PF_6)_2$, while recrystallization of the fraction only soluble in hot acetonitrile provides unexpectedly the HSO_4^- salt of the dicationic complex whose formula is determined as $(\mathbf{Mo_2B})_3(HSO_4)_6^{\bullet}(H_2O)_4$.

$(\mathbf{Mo_2B})(PF_6)_2$ crystallizes in the monoclinic system, space group $P2_1/c$ with two independent molecules, each of them located on an inversion center (Figure 7a). They both exhibit a chair conformation with a dihedral angle within the metallacycles along the S–S hinge of 34.6(4)° and 39.2(1)°. Relevant bond angles and bond lengths within the metallacycles are reported in Table 2 together with those of the neutral and mononuclear **MoB** and $Cp_2Mo(bdt)$ complexes for comparison. The less soluble $(\mathbf{Mo_2B})_3(HSO_4)_6\cdot(H_2O)_4$ salt crystallizes in the triclinic system, space group $P\bar{1}$, with one bimetallic complex located on an inversion center and another one in general position (Figure 7b). The one located on the inversion center exhibits a chair conformation with a dihedral angle along the S–S hinge of 34.7(4)°. The other crystallographically independent complex in general position exhibits a boat conformation,

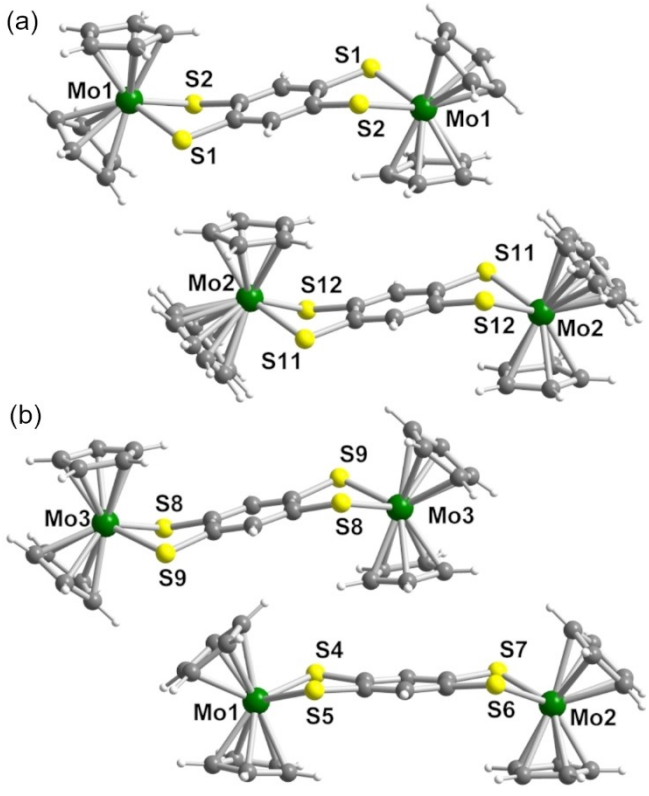

Figure 7. Molecular structures of the dicationic $\mathbf{Mo_2B^{2+}}$ complexes in (a) $(\mathbf{Mo_2B})(PF_6)_2$ with two complexes on inversion centers with chair conformation and, (b) $(\mathbf{Mo_2B})_3(HSO_4)_6\cdot(H_2O)_4$ with one complex on inversion center with chair conformation (Mo3) and one complex in general position with boat conformation (Mo1,Mo2).

Table 2. Selected experimental bond distances (Å) and folding angle θ (°) within the metallacycles in **MoB** and $\mathbf{Mo_2B^{2+}}$.

Bond	$Cp_2Mo(bdt)$	MoB	Mo_2B^{2+} in $[Mo_2B][PF_6]_2$ Complex Mo1	Complex Mo2	Mo_2B^{2+} in $[Mo_2B]_3[HSO_4]_6\bullet(H_2O)_4$ Complex Mo3	Complex Mo1Mo2
S–Mo	2.437(1) 2.437(1)	2.4345(8) 2.4346(9)	2.438(2) 2.424(2)	2.410(2) 2.423(2)	2.409(8) 2.428(10)	2.427(6) Mo1 2.425(9) Mo1 2.415(8) Mo2 2.413(9) Mo2
C–S	1.758(4) 1.762(4)	1.755(3) 1.760(3)	1.744(9) 1.731(9)	1.720(9) 1.737(9)	1.709(9) 1.723(8)	1.706(10) Mo1 1.703(9) Mo1 1.716(10) Mo2 1.710(9) Mo2
a	1.396(5)	1.406(4)	1.447(12)	1.444(11)	1.449(11)	1.450(11) Mo1
a′	1.388(5)	1.402(4)	1.447(12)	1.444(11)	1.449(11)	1.453(12) Mo2
b	1.402(5)	1.395(4)	1.386(12)	1.381(12)	1.410(11)	1.404(11) Mo1
b′	1.397(5)	1.399(4)	1.385(12)	1.396(12)	1.382(10)	1.387(10) Mo1
c	1.388(6)	1.391(4)	1.385(12)	1.396(12)	1.410(11)	1.384(11) Mo2
c′	1.389(6)	1.385(4)	1.386(12)	1.381(12)	1.382(10)	1.385(11) Mo2
Θ [a]	8.3(1)	10.4(2)	34.6(4)	39.2(1)	34.7(4)	21.4(4) Mo1 31.6(2) Mo2

[a] Folding angle of the metallacycle along the S–S hinge.

with the metallacycles distorted along the S–S hinge with two different dihedral angles of 21.4(4)° along S4-S5 (Mo1) and 31.6(2)° along S6—S7 (Mo2). Apart from these smaller folding angles, the bond lengths within the metallacycles are close to those observed in the PF_6^- salt. Three crystallographically independent HSO_4^- anions are found, one of them strongly disordered, together with two oxygen atoms attributed to water molecules. The hydrogen atoms of the anions and the water molecules could not be observed on the Fourier difference map but their solid-state organization (Figures S7-S8) is characterized by a hydrogen bonded network with O···O distances in a 2.4–2.8 Å range.

The observation of both chair and boat conformations in $\mathbf{Mo_2B^{2+}}$ structures confirms the geometry optimizations (see above) which indicated very small energy differences between them. The evolution of the bond distances within the metallacycles in both salts (Table 2) follows the expected trends observed in mononuclear complexes[23] and simulated here for $\mathbf{Mo_2B^{0,1+,2+}}$ (see above), i.e. the lengthening of the C=C bond and shortening of the C–S bonds. Also, the ring in $\mathbf{Mo_2B^{2+}}$ adopts a more quinoid structure.

The dicationic state of $\mathbf{Mo_2B^{2+}}$ in these salts is further confirmed by the UV-vis-NIR absorption of an acetonitrile solution of the $(\mathbf{Mo_2B})(PF_6)_2$ crystals (Figure S9) which exhibits a broad NIR absorption band centered at 1158 nm and a narrower absorption band at 688 nm, fully consistent with the spectral signature of the dicationic species determined from the spectroelectrochemical measurements performed in DMSO and observed at 1204 and 711 nm (Figure 4b). The small observed shift is due to the use of acetonitrile instead of DMSO. Also, while the full characterization of the five expected oxidation states of **Mo_2B** had not been possible from CV experiments on the neutral complex (Figure S2), the isolation of these soluble dicationic salts allows us to investigate now their redox behavior at higher potentials by cyclic voltammetry in CH_3CN. Following the two redox processes associated with the $0/+1$ and $+1/+2$ charge changes, two extra redox processes can now be observed at higher potentials at $+1.05$ and $+1.57$ V vs. SCE (Figure S10), corresponding to the sequential oxidation to the tricationic and tetracationic state (Table 1), and confirming that the bimetallic **Mo_2B** complex can indeed exist under five different redox states.

Magnetic susceptibility measurements were performed down to 3 K on the $(\mathbf{Mo_2B})(PF_6)_2$ crystals. The salt exhibits a weak paramagnetic response well fitted with a Curie Weiss behavior in the whole temperature range, corresponding to 4.3 % $S = {}^1/_2$ radical species (Figure S11). These data indicate unambiguously that the dicationic complex is essentially in a singlet state at RT and below. The EPR spectrum of crystals of $(\mathbf{Mo_2B})(PF_6)_2$ solubilized in CH_3CN displays a signal at $g = 2.0123$ consistent with the presence of an organic radical (Figure S12). The absence of any half-field signal around 1600–1700 Gauss in the frozen glass spectrum (66 K) confirms that $\mathbf{Mo_2B^{2+}}$ has a singlet ground state rather than a triplet one, in agreement with the theoretical calculations. These observations are reminiscent of those reported on organic diradicals such as benzo-1,2:4,5-bis(1,3,2-dithiazolyl)[24] or dibenzofluoreno[3,2-b]fluorene.[25] In the former, the two spin states, triplet and diradical singlet, are also very close in energy.

Conclusions

In conclusion, we have reported the synthesis, characterization and DFT calculations of an original bimetallic complex involving two redox active molybdenocene/dithiolene moieties fused to a

benzo linker, namely **Mo_2B**. Electrochemical investigations demonstrate that **Mo_2B** be sequentially oxidized by 1e- steps up to the tetracationic state. Spectroelectrochemical investigations assisted by DFT calculations disclosed that the mono-oxidized and the bis-oxidized state can exist under different conformations, i.e. planar, boat and chair one for the cation radical species and boat and chair conformation for the bis-oxidized species. The existence of these various conformers is responsible for their unique NIR absorption properties. X-ray structure analyses together with spectroscopic investigations corroborate the existence of these various conformations. Interestingly, the bis-oxidized state exhibits a pronounced diradicaloid character as evidenced by EPR and magnetometry measurements corroborated by computational studies. Such diradicaloid systems are currently raising a strong interest for their possible applications in molecular electronics, spintronics and magnetics.[26] They are also motivating extended theoretical investigations aimed at understanding their structures and reactivity.[27] The new example provided here based on benzene tetrathiolate complements for the first time the numerous, analogous oxygen-based systems built on 2,5-dihydroxy-1,4-benzoquinone.[28]

Experimental Section

Materials and Methods: Chemicals and materials from commercial sources were used without further purification. All the reactions were performed under an argon atmosphere. NMR spectra were obtained in $CDCl_3$ unless indicated otherwise. Chemical shifts are reported in ppm, ^{1}H NMR spectra were referenced to residual $CHCl_3$ (7.26 ppm) and ^{13}C NMR spectra were referenced to $CHCl_3$ (77.2 ppm).Melting points were measured on a Kofler hot-stage apparatus and are uncorrected. Mass spectra were recorded by the Centre Régional de Mesures Physiques de l'Ouest, Rennes. Methanol, acetonitrile and dichloromethane were dried using Inert pure solvent column device. CVs were carried out on a 10^{-3} M solution of complex in CH_2Cl_2-$[NBu_4][PF_6]$ 0.1 M. CVs were recorded on a Biologic SP-50 instruments at 0.1 Vs^{-1} on a platinum disk electrode. Potentials were measured versus KCl Saturated Calomel Electrode (SCE). The spectroelectrochemical setup was performed in CH_2Cl_2-$[NBu_4][PF_6]$ 0.2 M using a Pt grid as the working electrode, a Pt wire as the counter electrode and SCE reference electrode. A Shimadzu 3600 plus spectrophotometer was used to record the UV-vis-NIR spectra. X-band EPR spectra were recorded on a Bruker EMX spectrometer.

*Synthesis of **Mo_2B** and **MoB***: Under inert atmosphere and using Schlenk techniques, a solution of NaOMe (freshly prepared from sodium (80 mg, 3.48 mmol) in 8 mL of dry methanol) was added to a Schlenk tube containing the benzo proligand **1** (200 mg, 0.76 mmol). The reaction was stirred for 2 h at room temperature, then Cp_2MoCl_2 (457 mg, 1.54 mmol) was added and the reaction was stirred overnight at room temperature. 10 mL of water was added to the reaction mixture and the organic solvent was removed under vacuum. The red/brown precipitate was filtered and washed successively with water, ethanol and diethylether. This brown precipitate was a mixture between **MoB** and **Mo_2B**. To isolate each of them, the red/brown precipitate was washed several times with dichloromethane until the filtrate change from red to colorless. The red filtrate was evaporated under vacuum and **MoB** was obtained as a red powder in 10% yield. Crystals of sufficient quality for X-ray diffraction were obtained by slow evaporation of a dichloromethane solution: m.p. $>260\,^{\circ}C$; ^{1}H NMR (300 MHz, $CDCl_3$) $\delta = 7.41$ (s; 2H), 5.32 (s; 10H). ^{13}C NMR (75 MHz, $CDCl_3$) $\delta = 146.5$, 124.8, 121.2 (phenyl-CH), 98.4 (Cp); IR: $\upsilon_{C=O} = 1614\ cm^{-1}$; HRMS (ESI): m/z calcd for $C_{17}H_{13}OS_4Mo$ $[M+H]^+$: 458.88978; found 458.8893 (1 ppm).

The brown poorly soluble precipitate, identified as the **Mo_2B** complex was obtained in 43% yield. m.p. $>260\,^{\circ}C$; ^{1}H NMR (300 MHz, DMSO) $\delta = 6.89$ (s; 2H), 5.31 (s; 20H). ^{13}C NMR (75 MHz, DMSO) $\delta = 139.7$, 125.8, 98.6 (Cp); HRMS (ESI) calcd for $C_{26}H_{22}S_4Mo_2$ $[M^{+\cdot}]$ 657.8707; found 657.873 (4 ppm).

Synthesis of $Cp_2Mo(bdt)$. To a Schlenck tube containing a suspension of benzene-1,2-dithiol (50 mg, 0.35 mmol) and Cp_2MoCl_2 (105 mg, 0.35 mmol) in dry and degassed toluene (10 mL), Et_3N (0.1 mL, 0.71 mmol) and H_2O (2 mL) were added successively and the solution was stirred under reflux for 1 h, turning from green to dark red. After cooling down at room temperature, the organic layer was separated and washed with water, dried with $MgSO_4$, and the solvent was removed under vacuum. Purification by column chromatography (CH_2Cl_2) afforded $Cp_2Mo(bdt)$ as a red powder (46%, 60 mg, 0.16 mmol). m.p. $>260\,^{\circ}C$; ^{1}H NMR (300 MHz, DMSO) $\delta = 7.11$ (dd, $J = 5.7$, 3.2 Hz, 2H), 6.54 (dd, $J = 5.7$, 3.2 Hz, 2H), 5.36 (s, 10H); ^{13}C NMR (75 MHz, DMSO) $\delta = 146.3$, 127.4, 120.8, 98.2; HRMS (ESI) calcd for $C_{26}H_{22}S_4Mo_2$ $[M^{+\cdot}]$ 657.8707; found 657.873; elem. analysis calcd (%) for $[C_{16}H_{14}S_2Mo_+CH_2Cl_2]$: C, 45.25; H, 3.57; S, 14.21; found: C, 45.34; H, 3.48; S, 16.17.

X-ray Crystallography: Suitable crystals for X-ray diffraction single crystal experiments were selected and mounted with a cryoloop on the goniometer head of a D8 Venture (Bruker-AXS) diffractometer equipped with a CMOS-PHOTON70 detector, using Mo–Kα radiation ($\lambda = 0.71073$ Å, multilayer monochromator). Structures were solved by dual-space algorithm using SHELXT program, [29] and then refined with full-matrix least-squares methods based on F^2 (*SHELXL*) program. [30] All non-hydrogen atoms were refined with anisotropic atomic displacement parameters. H atoms (except those on H_2O molecules and HSO_4^- anion) were finally included in their calculated positions and treated as riding on their parent atom with constrained thermal parameter. Details of the final refinements are summarized in Table S3.

Deposition Number(s) 2241773 (for $Cp_2Mo(bdt)$), 2241774 (for **MoB**), 2241775 (for $(\mathbf{Mo_2B})(PF_6)_2$), 2241776 (for $(\mathbf{Mo_2B})_3(HSO_4)_6{\cdot}(H_2O)_4$) contain(s) the supplementary crystallographic data for this paper. These data are provided free of charge by the joint Cambridge Crystallographic Data Centre and Fachinformationszentrum Karlsruhe Access Structures service.

Computational details: DFT calculations were performed using ORCA 5.0 program package[31] at the B3LYP-D3/def2-TZVP level. Geometry optimizations were followed by frequency calculations to ensure the validity of the minima. UV-Visible absorption spectra were obtained with TD-DFT calculations, computing the first 35 electronic transitions. In addition, RIJCOSX approximations were used to accelerate the SCF procedures.[32] In all steps, solvent (DMSO) effects were included through a Polarizable Continuum Model (PCM).[33]

Supporting Information

Figures S1–S19 and Tables S1–S3.

Acknowledgements

Financial support was obtained from ANR (Paris France) under contracts n°19-CE08-0029-02 and n°20-CE09-0002-01, and a PhD grant (to K. Youssef) from Région Bretagne. This work was granted access to the HPC resources of TGCC/CEA/CINES/IDRIS under the allocations 2022-AD010805032R1, A0100800649 and AD010800649R1 awarded by GENCI. We thank Olivier Jeannin (Rennes) for his help in the X-ray analyses and Thierry Guizouarn (Rennes) for the magnetic susceptibility (SQUID) measurements.

Conflict of Interests

There are no conflict of interest to declare.

Data Availability Statement

The data that support the findings of this study are available in the supplementary material of this article.

Keywords: metallocenes · molybdenum · radical ions · S ligands · through-bond interactions

[1] R. Matsuoka, R. Sakamoto, T. Kambe, K. Takada, T. Kusamoto, H. Nishihara, *Chem. Commun.* **2014**, *50*, 8137–8139.
[2] B. Liu, W. Qiao, Z. Y. Wang, *RSC Adv.* **2015**, *5*, 6815–6822.
[3] W. Shi, G. Wu, K. Hippalgaonkar, J. S. Wang, J. Xu, S. W. Yang, *J. Am. Chem. Soc.* **2018**, *140*, 13200–13204.
[4] a) R. Eisenberg, H. Gray, *Inorg. Chem.* **2011**, *50*, 9741–9751; b) G. Periyasamy, N. A. Burton, I. H. Hillier, M. A. Vincent, H. Disley, J. McMaster, C. D. Garner, *Faraday Discuss.* **2007**, *135*, 469–488.
[5] L. Chen, M. Wang, F. Gloaguen, D. Zheng, P. Zhang, L. Sun, *Chem. Eur. J.* **2012**, *18*, 13968–13973.
[6] a) K. Arumugam, R. Yu, D. Villagrán, T. G. Gray, J. T. Mague, J. P. Donahue, *Inorg. Chem.* **2008**, *47*, 5570–5572; b) K. Arumugam, M. C. Shaw, P. Chandrasekaran, D. Villagrán, T. G. Gray, J. T. Mague, J. P. Donahue, *Inorg. Chem.* **2009**, *48*, 10591–10607.
[7] M. Murata, S. Kaji, H. Nishimura, A. Wakamiya, Y. Murata, *Eur. J. Inorg. Chem.* **2016**, 3228–3232.
[8] C. Hua, J. A. DeGayner, T. D. Harris, *Inorg. Chem.* **2019**, *58*, 7044–7053.
[9] a) H. Köpf, H. Balz, *J. Organomet. Chem.* **1990**, *387*, 77–81; b) H. Balz, H. Köpf, J. Pickardt, *J. Organomet. Chem.* **1991**, *417*, 397–406.
[10] M. Nomura, M. Fourmigué, *Inorg. Chem.* **2008**, *47*, 1301–1312.
[11] B. H. Zhu, Y. Shibata, S. Muratsugu, Y. Yamanoi, H. Nishihara, *Angew. Chem. Int. Ed.* **2009**, *48*, 3858–3861; *Angew. Chem.* **2009**, *121*, 3916–3919.
[12] A. L. Whalley, A. J. Blake, D. Collison, E. S. Davie, H. J. Disley, M. Helliwell, F. E. Mabbs, J. McMaster, C. Wilson, C. D. Garner, *Dalton Trans.* **2011**, *40*, 10457–10472.
[13] A. J. Taylor, E. S. Davies, J. A. Weinstein, I. V. Sazanovich, O. V. Bouganov, S. A. Tikhomirov, M. Towrie, J. McMaster, C. D. Garner, *Inorg. Chem.* **2012**, *51*, 13181–13194.
[14] a) M. Fourmigué, *Acc. Chem. Res.* **2004**, *37*, 179–186; b) M. Fourmigué, *Coord. Chem. Rev.* **1998**, *178–180*, 823–864.
[15] a) A. Vacher, Y. Le Gal, T. Roisnel, V. Dorcet, T. Devic, F. Barrière, D. Lorcy, *Organometallics* **2019**, *38*, 4399–4408; b) K. Youssef, A. Vacher, F. Barrière, T. Roisnel, D. Lorcy, *Polyhedron* **2022**, *226*, 116086.
[16] M. Abe, *Chem. Rev.* **2013**, *113*, 7011–7088.
[17] J. Larsen, K. Bechgaard, *J. Org. Chem.* **1987**, *52*, 3285–3288.
[18] A. Kutoglu, H. Köpf, *J. Organomet. Chem.* **1970**, *25*, 455–460.
[19] a) K. Lahlil, A. Moradpour, C. Bowlas, F. Menou, P. Cassoux, J. Bonvoisin, J. P. Launay, G. Dive, D. Dehareng, *J. Am. Chem. Soc.* **1995**, *117*, 9995–10002; b) X. Gao, W. Wu, Y. Liu, S. Jiao, W. Qiu, G. Yu, L. Wang, D. Zhu, *J. Mater. Chem.* **2007**, *17*, 736–743; c) U. Scherer, Y. J. Shen, M. Adam, W. Bietsch, J. U. von Schütz, K. Müllen, *Adv. Mater.* **1993**, *5*, 109–112; d) M. Adam, A. Bohnen, V. Enkelmann, K. Müllen, *Adv. Mater.* **1991**, *3*, 600–602.
[20] J. K. Hsu, C. J. Bonangelino, S. P. Kaiwar, C. M. Boggs, J. C. Fettinger, R. S. Pilato, *Inorg. Chem.* **1996**, *35*, 4743–4751.
[21] T. Soda, Y. Kitagawa, T. Onishi, Y. Takano, Y. Shigeta, H. Nagao, Y. Yoshioka, K. Kamaguchi, *Chem. Phys. Lett.* **2000**, *319*, 223–230.
[22] U. Jahn, P. Hartmann, I. Dix, P. G. Jones, *Eur. J. Org. Chem.* **2001**, 3333–3355.
[23] a) M. Fourmigué, B. Domercq, I. V. Jourdain, P. Molinié, F. Guyon, J. Amaudrut, *Chem. Eur. J.* **1998**, *4*, 1714–1723; b) R. Clérac, M. Fourmigué, J. Gaultier, Y. Barrans, P. A. Albouy, C. Coulon, *Eur. Phys. J. B* **1999**, *9*, 431–443; c) R. Clérac, M. Fourmigué, C. Coulon, *J. Solid State Chem.* **2001**, *159*, 413–419.
[24] a) E. Dormann, M. J. Nowak, K. A. Williams, R. O. Angus, F. Wudl, *J. Am. Chem. Soc.* **1987**, *109*, 2594–2599; b) T. M. Barclay, A. W. Cordes, R. H. de Laat, J. D. Goddard, R. C. Haddon, D. Y. Jeter, R. C. Mawhinney, R. T. Oakley, T. T. M. Palstra, G. W. Patenaude, R. W. Reed, N. P. C. Westwood, *J. Am. Chem. Soc.* **1997**, *119*, 2633–2641.
[25] H. Hayashi, J. E. Barker, A. C. Valdivia, R. Kishi, S. N. MacMillan, C. J. Gomez-Garcia, H. Miyauchi, Y. Nakamura, M. Nakano, S. Kato, M. M. Haley, J. Casado, *J. Am. Chem. Soc.* **2020**, *142*, 20444–20455.
[26] a) I. Ratera, J. Veciana, *Chem. Soc. Rev.* **2012**, *41*, 303–349; b) X. Hu, W. Wang, D. Wang, Y. Zheng, *J. Mater. Chem. C* **2018**, *6*, 11232–11242.
[27] T. Stuyver, B. Chen, T. Zeng, P. Geerlings, F. De Proft, R. Hoffmann, *Chem. Rev.* **2019**, *119*, 11291–11351.
[28] a) R. Maskey, T. Thorwart, S. E. Ebel, A. Jocic, D. Hartman, L. Greb, *Chem. Eur. J.* **2023**, *29*, e202300269 (1-5); b) M. E. Ziebel, C. A. Gaggioli, A. B. Turkiewicz, W. Ryu, L. Gagliardi, J. R. Long, *J. Am. Chem. Soc.* **2020**, *142*, 2653–2664; c) S. Kitagawa, S. Kawata, *Coord. Chem. Rev.* **2002**, *224*, 11–34.
[29] G. M. Sheldrick, *Acta Crystallogr.* **2015**, *A71*, 3–8.
[30] G. M. Sheldrick, *Acta Crystallogr.* **2015**, *C71*, 3–8.
[31] F. Neese, F. Wennmohs, U. Becker, C. Riplinger, *J. Chem. Phys.* **2020**, *152*, 224108.
[32] F. Neese, F. Wennmohs, A. Hansen, U. Becker, *Chem. Phys.* **2009**, *356*, 98–109.
[33] M. Garcia-Ratés, F. Neese, *J. Comput. Chem.* **2020**, *41*, 922–939.

Manuscript received: February 22, 2023
Accepted manuscript online: May 23, 2023
Version of record online: July 8, 2023